

Description of Solid-to-Solid Redox Processes Based on the Voltammetry of Immobilized Particles Methodology: A Logistic Approximation

Antonio Doménech-Carbó*



Cite This: *J. Phys. Chem. C* 2022, 126, 11822–11832



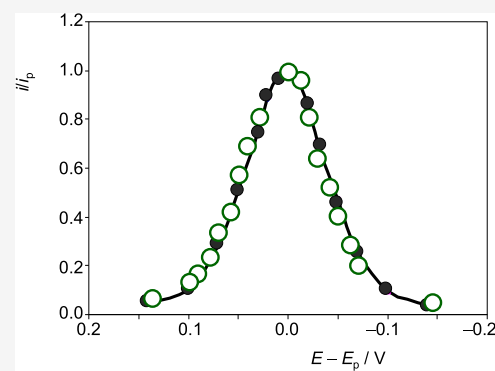
Read Online

ACCESS |

Metrics & More

Article Recommendations

ABSTRACT: A semiempirical model to describe the voltammetry of non-topotactic solid-to-solid redox processes occurring in the voltammetry of immobilized particles (VIMP) electrochemistry is described. It is applied to the reduction of solid metal compounds to the corresponding metal in contact with suitable electrolytes. The model is based on the assumption that the transferred charge is a logistic function of the applied potential, a situation that applies for reversible redox processes involving strongly adsorbed reactants. The model satisfactorily applies to reproduce linear potential scan curves recorded for graphite electrodes modified with different lead compounds (PbO, PbCl₂·2H₂O, lead-tin yellow, lead white) in contact with 0.10 M H₂SO₄ aqueous solution.



1. INTRODUCTION

The voltammetry of species confined to electrode surfaces is of crucial importance in electrochemistry.^{1,2} Theoretical models have been focused on different types of adsorption isotherms and degree of electrochemical reversibility.^{3–5} The electrochemistry of surface-confined species, however, is not limited to adsorbates, and theoretical studies include nanoparticles⁶ and droplets⁷ anchored to—or impacting onto—electrodes, porous electrodes,⁸ and microparticulate deposits of insulating or semiconducting solids.⁹ Recently, interactions between immobilized redox centers,^{10,11} semiconductor electrode voltammetry¹² giving rise to phase transitions,¹³ and charge transfer in solid-state redox processes¹⁴ have been treated.

Much research in solid-state electrochemistry has been developed by application of the voltammetry of immobilized particles (VIMP), a solid-state electrochemical technique developed by Scholz et al.¹⁵ that provides analytical information on sparingly soluble nonconducting solids via their abrasive transference to inert electrodes.^{16,17} The VIMP mainly involves three types of processes, topotactic solid-state transformation accompanied by ion intercalation/deintercalation, reductive/oxidative dissolutions of solids, and solid-to-solid transformations with segregation of different phases. The first group of processes, of obvious importance for electrointercalation, has been modeled under conditions of reversibility and diffusion control.^{18–23} The modeling of reductive/oxidative dissolution of nonconducting solids was based on the kinetics of solid-state reactions.^{24,25} The third group of processes, however, has received much less attention, theoretical modeling being

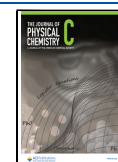
limited to that developed by Jaworski et al.²⁶ for the reduction of silver halides to silver. This model assumes that mixed metal salt/metal crystals are formed during the voltammetric experiments and provides numerical simulations of linear potential scan voltammograms in satisfactory agreement with experimental data.

Much solid-to-solid redox processes are topotactic transformations, i.e., does not involve structural changes in the solid phase during electrochemical cycles. In general, however, this type of process involves nontopotactic transformations where structurally different phases are formed following a complex electrochemical pathway. Given the importance of such processes in mineralogical^{15–17} and archaeometric^{27,28} analysis, including metal dating,^{29–31} the disposal of analytical models reproducing voltammetric curves is of interest in these research fields, in particular, to characterize different solid compounds.^{16,17} Here, an operational, semiempirical approach based on the modeling of the charge transfer process in terms of logistic equations is described. These equations were introduced by Verhulst in the 19th century to describe population growth³² and have been further expanded to describe

Received: May 3, 2022

Revised: June 7, 2022

Published: July 8, 2022



not only social phenomena but also a variety of biological and physicochemical phenomena.³³ A common characteristic of these phenomena is the existence of size limitation of the growing system, just a property of solid-to-solid electrochemical processes. For our purposes, the essential idea is that the complex pathway involved in this kind of process can in principle be modeled in terms of solid-state reaction kinetics, one of whose possible mathematical formulations is logistic. The flexible nature of the logistic equations and their suitability to provide analytical (rather than numerical) voltammetric curves favor their use for modeling the aforementioned solid-state processes.

This view is consistent with the proposal of logistic equations to model electroinsertion processes in inorganic films.^{34,35} Although the validity of this approach for replacing conventional electrodynamic equations was questioned,³⁶ the modeling presented here can be seen as an operational approach able to provide theoretical voltammetric curves in satisfactory agreement with experimental data. A series of lead compounds, namely, litharge (yellow PbO), massicot (red-yellow PbO), lead white ($2\text{PbCO}_3 \cdot \text{Pb}(\text{OH})_2$), $\text{PbCl}_2 \cdot 2\text{H}_2\text{O}$, Naples yellow ($\text{Pb}_2\text{Sb}_2\text{O}_7$), and type II lead-tin yellow ($\text{Pb}(\text{Sn},\text{Si})\text{O}_3$), was selected for testing the model. These compounds are of interest by their historical use as pigments and their widely studied electrochemistry in contact with aqueous electrolytes.^{16,17,27–29,37}

2. EXPERIMENTAL SECTION

Litharge (Carlo Erba), Massicot (Kremer 43010), $\text{PbCl}_2 \cdot 2\text{H}_2\text{O}$ (Carlo Erba), lead-tin yellow of type II (Kremer 10120), Naples yellow (light yellow, Kremer 43125), and lead white (Cremnitz white, Kremer 46002) were used. Voltammetric measurements were carried out at microparticulate deposits of the lead compounds on commercial paraffin-impregnated graphite bars (Alpino Maxim HS type, 2 mm diameter) in contact with 0.10 M H_2SO_4 (Probus) aqueous solution. A conventional three-electrode cell connected to a CH 660c potentiostat was used. The electrolyte solution was deoxygenated by bubbling Ar 10–15 min prior to voltammetric measurements. Electrode modification was performed by pressing the graphite bar, previously polished over paper, as described in ref 16, over a fine layer of the solid distributed onto the plane face of an agate mortar. Then, the electrode was put into contact with the electrolyte solution and electrochemical measurements were carried out using linear potential scan voltammetry (LSV).

3. RESULTS AND DISCUSSION

3.1. Voltammetric Response. Figure 1 shows the LSVs recorded at litharge-modified graphite electrodes in contact with 0.10 M H_2SO_4 aqueous solution at potential scan rates of 1, 5, 10, and 20 mV s^{-1} . At low scan rates, a sharp cathodic peak is recorded with almost symmetrical ascending and descending branches in the current/potential curve. Upon increasing the sweep rate, the cathodic signal becomes negatively shifted and displays a progressively less acute descending branch.

Figure 2a illustrates the variation of the peak potential (E_p) with the logarithm of potential scan rate ($\ln \nu$) in LSVs at sweep rates between 1 and 60 mV s^{-1} . The peak potential shifts negatively on increasing ν yielding a curved E_p vs $\ln \nu$ representation. In turn, the peak currents increase on increasing potential scan rate, as shown in Figure 2b. Under our experimental conditions, the peak potential recorded in replicate

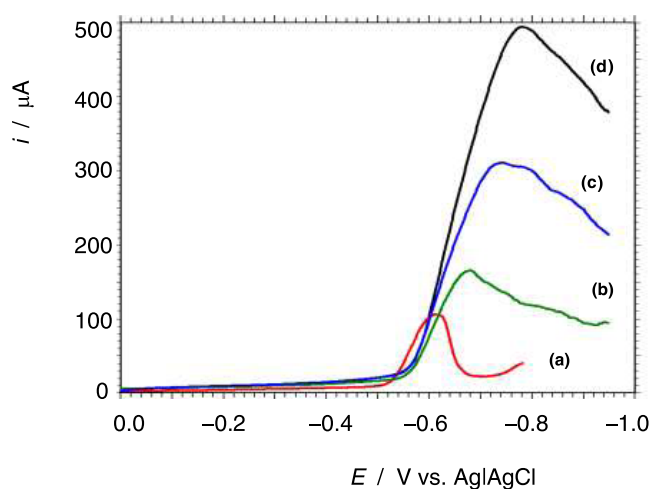


Figure 1. Cathodic LSVs of microparticulate deposits of litharge onto graphite electrode in contact with 0.10 M H_2SO_4 aqueous solution at potential scan rates of (a) 1, (b) 5, (c) 10, and (d) 20 mV s^{-1} .

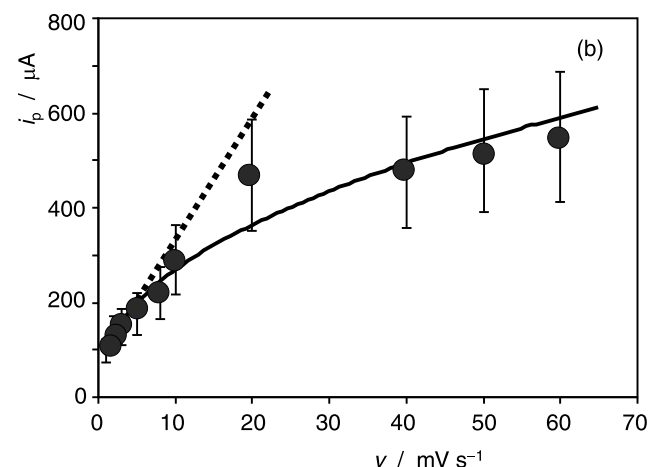
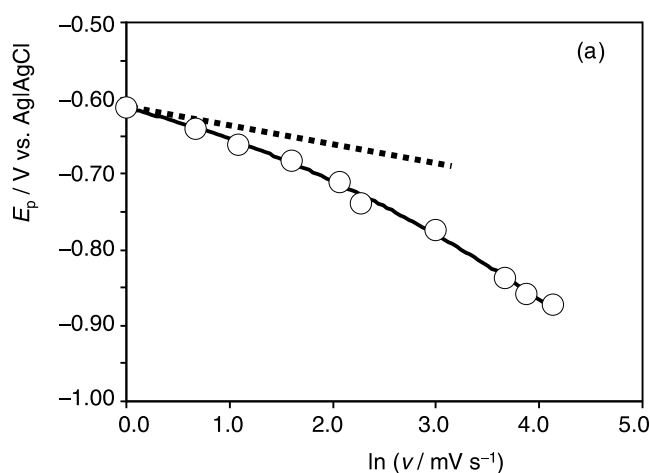
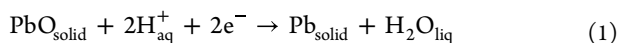


Figure 2. Variation of (a) peak potential (E_p) with $\ln \nu$ and (b) peak current (i_p) with ν , in cathodic LSVs of microparticulate deposits of litharge onto graphite electrode in contact with 0.10 M H_2SO_4 aqueous solution. Averaged values from three independent replicate experiments are represented. Continuous lines represent the polynomial fit of the entire set of experimental data, while dotted lines correspond to the asymptotic straight line at 1 mV s^{-1} (a) and the linear fit of data between 1 and 5 mV s^{-1} (b).

experiments at a given potential scan rate remains essentially constant (maximum dispersion in ± 10 mV), but the peak currents display variations between 10 and 25% in replicate measurements. This is due to the fact that, in this type of experiments, performed by means of the usual VIMP abrasive conditioning of the electrode, the net amount of solid transferred onto the graphite electrode cannot be controlled. Despite this relatively large uncertainty, it appears that peak currents increase linearly with potential scan rate between 1 and 5 mV s^{-1} .

3.2. Electrochemical Pathway. Conjointly considered, the above data suggest that there is a change in the electrochemical pathway depending on the time scale of the experiment. Overall, the electrochemical reduction of a microparticulate deposit of lead oxide can be represented as



This process was described by Hasse and Scholz³⁵ in terms of the topotactic PbO-to-Pb transformation mediated by proton insertion resulting in the formation of an ionophoric intermediate layer as schematically depicted in Figure 3.

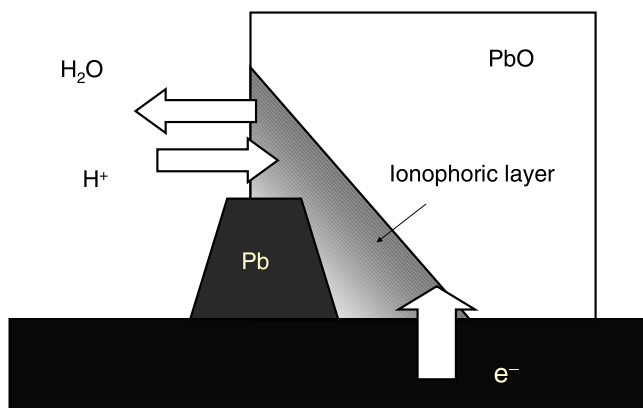
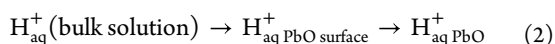


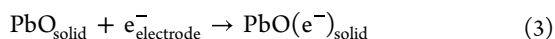
Figure 3. Schematic for the proton-assisted topotactic reduction of PbO to Pb under conditions of typical VIMP experiments in contact with aqueous electrolytes.

Formally, this process can be divided into different elementary steps, namely:

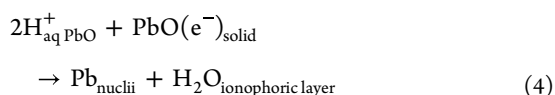
- (a) Proton diffusion from the bulk solution to the PbO particle surface followed by insertion and transport into the solid lattice forming an ionophoric layer



- (b) Electron injection and transport into the solid coupled, by reasons of charge conservation, to proton insertion



- (c) Formation of metal nuclii segregated from the ionophoric layer



- (d) Growth and coalescence of metallic nuclii forming a microparticulate deposit of lead crystals

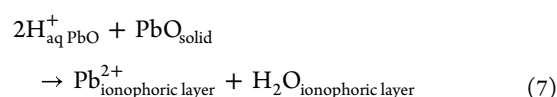


- (e) Water release from the ionophoric layer

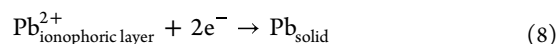


The above equations summarize a first possible pathway (in the following, mechanism I) to interpret litharge to lead electrochemical reduction. Here, the rate-determining step will be the solid-state charge transfer described by eqs 3 and 4, necessarily coupled by reasons of charge conservation.

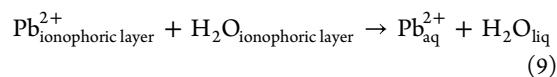
A second electrochemical pathway (mechanism II) can alternatively be proposed assuming that the electron transfer step involves “free” Pb^{2+} ions formed in the ionophoric layer. Then, after the processes represented by eq 2, there is a release of Pb^{2+} ions toward the ionophoric layer



These ions are subsequently reduced with the concomitant growth and coalescence of metallic nuclii



Alternatively, Pb^{2+} ions may pass into the electrolyte solution,



where they are reduced



In this second model, it is conceivable that the rate-determining step was the process described by eq 7. Ultimately, this process can be described in terms of interdiffusion of H^{+} and Pb^{2+} through the ionophoric layer.

This is a complex situation where different steps can be rate-determining depending on the composition of the electrolyte and the distribution of shape and size of solid particles of the parent compound on the electrode surface. Accordingly, the description in terms of the usual electrodynamic equations is considerably difficult. Available models refer to diffusive control of ion insertion,^{18–23} solid-state reaction kinetics,³⁸ and nucleation/growth models.³⁹ Two aspects, however, can be underlined: (a) Since the process involves a microparticulate deposit of PbO crystals, the charge transport must reach a maximum limiting value; (b) the flow of ions throughout the solid phase(s) has characteristics of a nonlinear, feedback-influenced dissipative process.^{34,35} As will be discussed below (*vide infra*), these two characteristics are consistent with the use of logistic formulations.

3.3. Theoretical Approach, Reversible Case. In the classical treatment² of surface-confined electron transfer processes, the Butler–Volmer kinetics for an n -electron transfer is expressed as

$$i(t) = nFAk[\Gamma_{\text{o}} e^{\beta F(E-E^{\circ})/RT} - \Gamma_{\text{rd}} e^{(1-\beta)F(E-E^{\circ})/RT}] \quad (11)$$

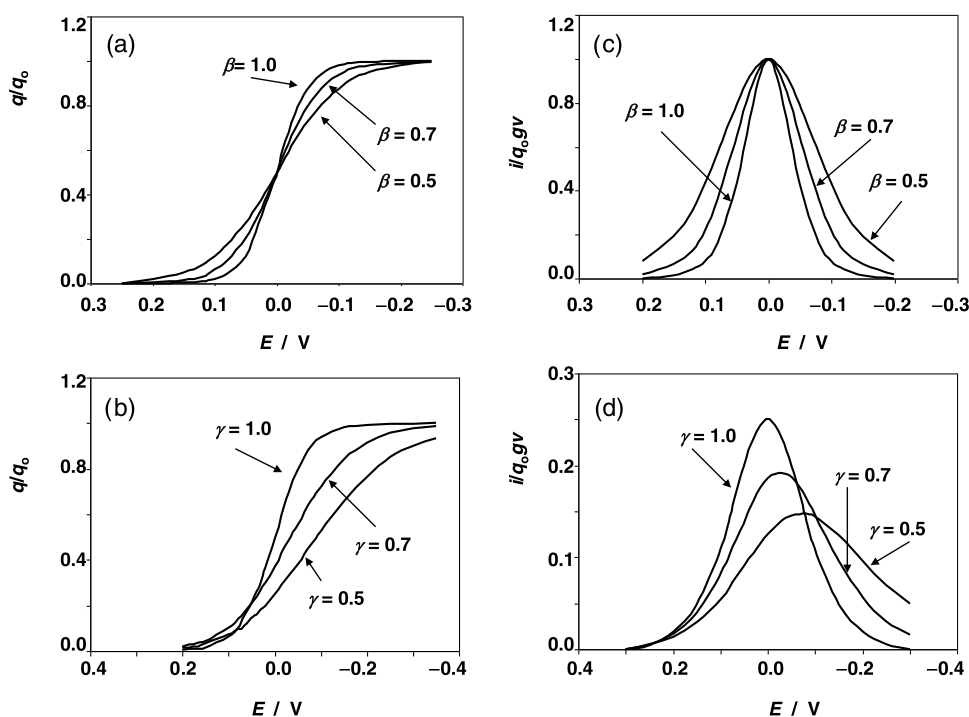


Figure 4. Theoretical (a, b) q/q_0 vs E and (c, d) $i/q_0\nu$ vs E voltammetric curves taking $E^{\circ'} = 0.0$ V. (a, c) Reversible case, current/potential curves from eqs 17 and 19 taking $g = \beta F/RT$ with $\beta = 1.0, 0.7,$ and 0.5 ; (b, d) general case, current–potential curves from eqs 23 and 24 taking $g = \beta F/RT$ with $\beta = 0.50$ and different values of γ .

where k is the rate constant of the electrochemical reaction (s^{-1}) and Γ_{ox} and Γ_{rd} are the surface concentrations of the oxidized and reduced forms of the electroactive species (mol cm^{-2}), respectively, A the electrode area (cm^2), and the other symbols have their customary significance. The coefficient β equals $n' + \alpha$, where n' is the number of electrons transferred before the rate-determining step and α ($0 < \alpha < 1$) is the electron transfer coefficient of the latter. The formal electrode potential of the redox couple, $E^{\circ'}$, has to be redefined. Following Laviron,⁴⁰ this quantity can be related to the standard potential, E° , and the Gibbs free energies of surface attachment of the oxidized and reduced forms, $\Delta G_{sa\ ox}^{\circ}$, $\Delta G_{sa\ rd}^{\circ}$ by means of the relationship,

$$E^{\circ'} = E^{\circ} + \left(\frac{\Delta G_{sa\ ox}^{\circ} - \Delta G_{sa\ rd}^{\circ}}{nF} \right) \quad (12)$$

The cathodic current is expressed in terms of the gradient of surface concentration as²

$$i(t) = -nFA \left(\frac{d\Gamma_{ox}}{dt} \right) \quad (13)$$

In the reversible case, the current–potential (i – E) voltammetric curves can be obtained merely by combining eq 13 with the Nernst equation and assuming $\Gamma_{ox} + \Gamma_{rd} = \Gamma$ (constant) and that the adsorption follows the Langmuir isotherm.⁴⁰ The general expression of the current in a voltammetric experiment performed at a potential scan rate ν when the system behaves reversibly is^{1–3}

$$i = \frac{n^2 F^2 A \Gamma \nu}{RT} \frac{e^{nF(E-E^{\circ'})/RT}}{[1 + e^{nF(E-E^{\circ'})/RT}]^2} \quad (14)$$

Remarkably, this solution is formally equivalent to that obtained assuming that the transferred charge varies with the

applied potential following a logistic growth. The logistic functions were originally introduced by Verhulst to describe the kinetics of the growth of a population tending to a limiting value or carrying capacity.^{32,33} This formulation can be used as a flexible mathematical tool replacing time with other quantities representative of the growth (or decay) of the physical system under study.⁴¹ Accordingly, the charge passed throughout a voltammetric experiment involving surface-confined species can be expressed as the ratio between the charge passed q at the potential E applied at a time t , and the limiting charge, q_0 ($x(E) = q(E)/q_0$). Then, the logistic equation can be written as

$$\frac{dx(E)}{dE} = gx(E)(1 - x(E)) \quad (15)$$

where g represents a constant parameter (in the following, logistic constant) representative of the rate of variation of q with E . In voltammetric experiments, q and E vary with time so that integration of eq 15 yields

$$\ln \left(\frac{q(t)/q_0}{1 - q(t)/q_0} \right) = gE(t) + H \quad (16)$$

with H being the integration constant. Taking $H = -gE^{\circ'}$, one can write

$$q = q_0 \frac{e^{g(E-E^{\circ'})}}{1 + e^{g(E-E^{\circ'})}} \quad (17)$$

The current (anodic/cathodic) will be

$$i(t) = \frac{dq(t)}{dt} = \frac{dq(t)}{dE} \frac{dE}{dt} = \pm \nu \frac{dq(t)}{dE} \quad (18)$$

Accordingly

$$i = q_0 g v \frac{e^{g(E-E^{\circ'})}}{[1 + e^{g(E-E^{\circ'})}]^2} \quad (19)$$

This equation is formally equivalent to eq 14 so that taking $g = nF/RT$, eq 19 equals eq 14. This means that, taking this value of the logistic constant g , the current/potential response is theoretically predicted assuming the logistic variation of charge with the applied potential is equivalent to that predicted from the Butler–Volmer (BV) kinetics. In this regard, it is pertinent to emphasize that, as discussed in detail by Compton et al.,⁴² the Butler–Volmer equation is “phenomenological” as far as it is not derived from a thermodynamic, fundamental theory such as the Marcus–Hush one.⁴³ The phenomenological character of the BV equation stems from being based on a linear free energy relationship, which is a phenomenological relationship. Similar phenomenological nature can be attributed to the different adsorption isotherms (Langmuir, Frumkin, etc.) used to reach eq 14 and their analogues.⁶ Accordingly, the introduction of the logistic approach is, in principle, formally reasonable although, obviously, it will need clarification of the underlying physicochemical meaning.

According to eq 19, the voltammogram consists of a symmetric i – E curve at a peak potential equal to the formal electrode potential ($E_p = E^{\circ'}$) and peak current equal to $vq_0g/4$. Then, the generalized voltammetric curves can be expressed as:

$$\frac{i}{i_p} = \frac{4e^{g(E-E^{\circ'})}}{[1 + e^{g(E-E^{\circ'})}]^2} \quad (20)$$

This equation allows us to obtain a family of voltammetric curves taking different values of the parameter g . Ideally, these curves can be expanded to include deviations from electrochemical reversibility taking $g = \beta F/RT$. This is based on the assumption that the quasi-reversible i – E curves can be expressed in terms of different values of the coefficient β . Figure 4 depicts the theoretical voltammetric curves in terms of i/q_0gv ratio vs E for three different values of β ($=\alpha + n'$). Of course, the logistic approximation retains its semiempirical character. Figure 4 reflects, simply, that theoretical reversible and nonreversible i – E curves can also be reproduced inserting the appropriate numerical parameters into the logistic equations.

3.4. Generalized Logistic Curves. In general, the kinetics of electrochemical solid-state transformations can be considered as parallel to that of solid-state reactions and, in particular, to that of the dissolution/precipitation of ionic solids. Roughly, the modeling of the solid-to-solid electrochemical transformation must account for deviations from reversibility in the electron transfer and the solid-state kinetics, as well as changes in the volume of the system under study. One simple way to incorporate such effects is the use of a variant of logistic growth proposed by Richards,⁴⁴

$$\frac{dx(E)}{dE} = g x(E) [1 - x(E)^\gamma] \quad (21)$$

where γ is an exponent whose value has to be decided by experiment. This coefficient condensates the effects due to deviations from reversibility, volume changes, and solid-state kinetic complications. Integration of eq 21 yields

$$\ln\left(\frac{x}{(1-x^\gamma)^{1/\gamma}}\right) = gE + H \quad (22)$$

Taking, as before, $H = -gE^{\circ'}$, one can write

$$q = q_0 \left[\frac{e^{\gamma g(E-E^{\circ'})}}{1 + e^{\gamma g(E-E^{\circ'})}} \right]^{1/\gamma} \quad (23)$$

Accordingly

$$i = q_0 g v \frac{e^{g(E-E^{\circ'})}}{[1 + e^{\gamma g(E-E^{\circ'})}]^{1/\gamma+1}} \quad (24)$$

The peak potential and peak current are

$$E_p = E^{\circ'} + \frac{\ln \gamma}{\gamma g} \quad (25)$$

$$i_p = \frac{q_0 g v e^{-\ln \gamma/\gamma}}{[1 + e^{-\ln \gamma}]^{1/\gamma+1}} \quad (26)$$

respectively. Then

$$\frac{i}{i_p} = \frac{e^{\ln \gamma/\gamma} (1 + e^{-\ln \gamma})^{1/\gamma+1} e^{g(E-E^{\circ'})}}{[1 + e^{\gamma g(E-E^{\circ'})}]^{1/\gamma+1}} \quad (27)$$

Equation 27 reduces to eq 20 when $\gamma = 1$. Extending the formal similarity between the “canonical” eqs 14 and 19, eq 24 can be equaled to eq 14 taking $g = \beta F/RT$ and $\gamma = 1$. Note that, in the generalized logistic formulation represented by eqs 24–27, the peak potential of the i – E curves differs from the formal electrode potential of the redox couple. Here, there is a progressive cathodic shift of the peak potential and a decrease of the peak current on decreasing γ . Figure 4b compares the theoretical q/q_0 vs E (a,b) and i/q_0gv vs E (c,d) graphs taking $E^{\circ'} = 0.0$ V eqs 17 and 19 taking $\beta = 1.0, 0.7$, and 0.5 and the general case, inserting $\beta = 0.50$ into eqs 23 and 24 and taking $\gamma = 1.0, 0.7$, and 0.5 .

3.5. Tafel-Type Analysis. In the initial portion of the voltammetric curve, when $E \gg E^{\circ'}$, eq 24 can be approximated by

$$\ln i = \ln(q_0 g v) + g(E - E^{\circ'}) \quad (28)$$

This corresponds to a linear variation of $\ln i$ with E , i.e., a Tafel-type relationship (note that, strictly, Tafel relationships apply for quasi-equilibrium conditions⁴⁵). When $E \ll E^{\circ'}$, eq 24 can be approximated by,

$$\ln i = \ln(q_0 g v) - \gamma g(E - E^{\circ'}) \quad (29)$$

In VIMP experiments, the net amount of solid transferred onto the electrode surface varies from one to another experiment. On the other hand, the formal potential is in general unknown so that, for practical purposes, it is convenient to express this dependence in terms of the peak potential. Then, the Tafel-type relationships in generalized form can be expressed as

$$\ln\left(\frac{i}{i_p}\right) = \ln(1 + e^{-\ln \gamma}) + g(E - E_p) \quad (30)$$

$$\ln\left(\frac{i}{i_p}\right) = \ln(1 + e^{-\ln \gamma}) + \frac{(1 + \gamma) \ln \gamma}{\gamma^2} - \gamma(E - E_p) \quad (31)$$

Contrary to eqs 28 and 29, the above equations are independent of the net amount of electroactive material transferred onto the electrode surface.

In the central region of the voltammetric curve, when $g(E - E^\circ) \rightarrow 0$, one can approximate $e^{g(E - E^\circ)} \approx 1 + g(E - E^\circ)$. As before, it is convenient to eliminate q_0 taking the i/i_p ratio and replacing the formal potential by the peak potential. In the central region of the voltammetric peak, the $(i_p - i)/i_p$ ratio can reasonably be approximated by the relationship

$$\frac{i_p - i}{i_p} \approx \left(\frac{e^{\ln \gamma / \gamma} (1 + e^{-\ln \gamma})}{2^{1/\gamma + 1}} \right) \left[2^{1/\gamma + 1} + \frac{\ln \gamma}{\gamma} - g(E - E_p) \right] \quad (32)$$

This equation defines a linear variation of the $(i_p - i)/i_p$ ratio with $E - E_p$, corresponding to the so-called modified Tafel-type analysis of voltammetric curves previously introduced to electrochemically characterize different solid compounds.⁴⁶

3.6. Comparison with Experimental Data. Figure 5 compares the experimental and theoretical LSVs for litharge-

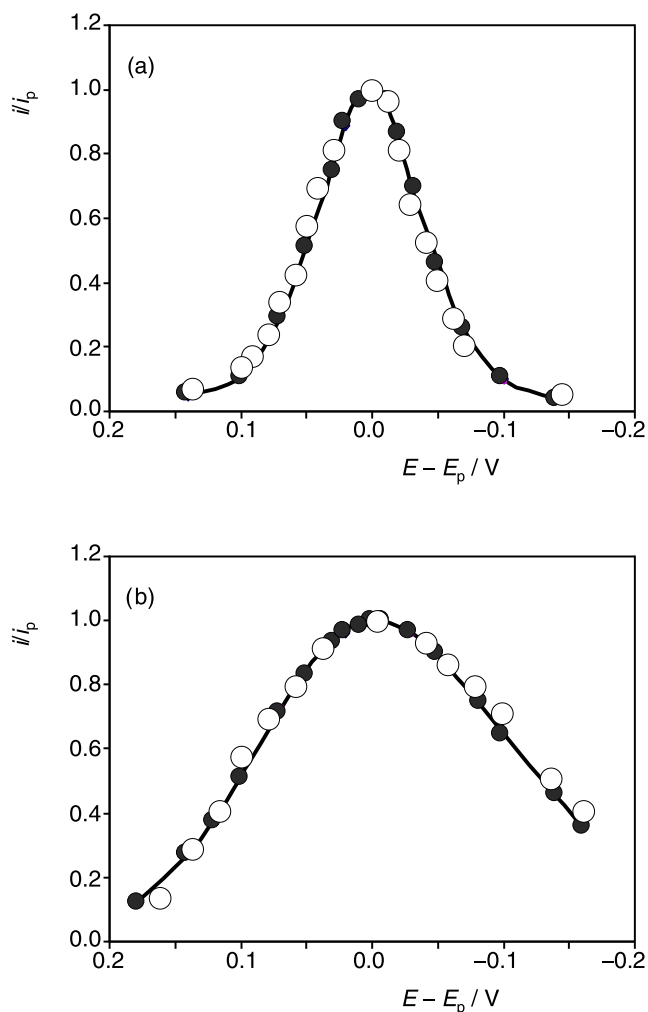


Figure 5. Superimposed experimental (circles) and theoretical (solid circles and continuous lines) LSVs for litharge-modified graphite electrodes in contact with 0.10 M H₂SO₄ at potential scan rates of (a) 2 and (b) 8 mV s⁻¹. Theory from eq 28 taking (a) $g = -34.9 \text{ V}^{-1}$, $\gamma = 1.05$; (b) $g = -31.5 \text{ V}^{-1}$, $\gamma = 0.40$.

modified graphite electrodes (normalized in terms of i/i_p vs $E - E_p$ representations) in contact with 0.10 M H₂SO₄ at potential scan rates of (a) 2 and (b) 8 mV s⁻¹. One can see that experimental data fit well to theoretical current/potential curves from eq 28 taking (a) $g = -34.9 \text{ V}^{-1}$, $\gamma = 1.05$, and (b) $g = -31.5 \text{ V}^{-1}$, $\gamma = 0.40$.

Our data (*vide infra*) clearly suggest that the values of the parameters g and γ significantly vary with the potential scan rate. Interestingly, the g values are near to those corresponding to the ideal case (at 298 K, 38.96 V⁻¹ for $n = 1$). This suggests the possibility of some correlation with the Laviron equation for the irreversible redox processes involving strongly adsorbed species² and the Brainina equation for the oxidative dissolution of metals,^{47,48} taking,

$$g = - \left(\frac{\beta F}{RT} \right) \ln \left(\frac{RTk_d}{\beta F v} \right) \quad (33)$$

where k_d is the rate constant for the electron transfer process depending not only on the composition of the electrolyte and the solid but also on factors such as the shape and size distribution of the solid particles.

Accordingly, eq 25 can be rewritten as,

$$E_p = E^\circ + \frac{\ln \gamma}{\gamma} \left[\left(\frac{\beta F}{RT} \right) \ln \left(\frac{RTk_d}{\beta F v} \right) \right]^{-1} \quad (34)$$

Equation 34 predicts a linear variation of E_p on $\ln v$ that, as judged by data in Figure 2a, diverges from experimental data obtained for litharge-modified electrodes. This relationship, however, is approximately valid to describe the E_p vs $\ln v$ data at scan rates below 10 mV s⁻¹. In turn, the generalized Tafel-type relationship at the foot of the voltammetric peak becomes

$$\ln \left(\frac{i}{i_p} \right) \approx \ln(1 + e^{-\ln \gamma}) - \left[\left(\frac{\beta F}{RT} \right) \ln \left(\frac{RTk_d}{\beta F v} \right) \right] (E - E_p) \quad (35)$$

Figure 6 shows $\ln(i/i_p)$ vs $E - E_p$ obtained for litharge at different potential scan rates. Experimental data satisfactorily fit with the expected linear relationship between these parameters,

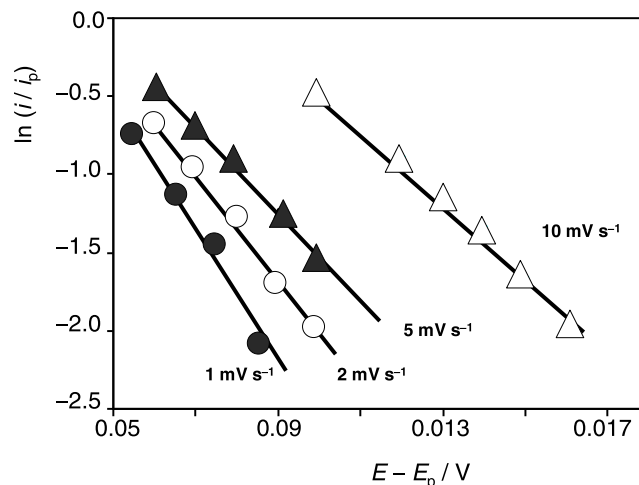


Figure 6. Plot of $\ln(i/i_p)$ vs $E - E_p$ obtained from data at the foot of the voltammetric waves recorded at litharge-modified graphite electrodes in contact with 0.10 M H₂SO₄ aqueous solution at different potential scan rates.

both the slope and the intercept varying with the potential scan rate. The corresponding slopes (T_S) are represented vs the logarithm of the potential scan rate in Figure 7. According to eq 35, such slopes must vary with potential scan rate as

$$T_S = -\left[\left(\frac{\beta F}{RT}\right)\ln\left(\frac{RTk_d}{\beta F}\right)\right] + \left(\frac{\beta F}{RT}\right)\ln v \quad (36)$$

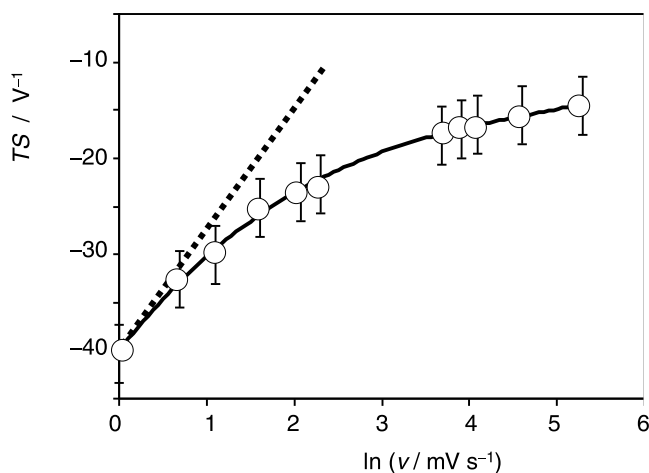


Figure 7. Variation of the Tafel slope (T_S) determined from data such as represented in Figure 6 with the logarithm of scan rate in the LSVs of litharge-modified graphite electrodes in contact with 0.10 M H_2SO_4 . The continuous line corresponds to the polynomial fit of data and the dotted line to the asymptotic straight line at low potential scan rates.

One can see here that, as is also suggested by peak potential and peak current data in Figure 2, the obtained data diverge from the expected linear dependence of T_S on $\ln v$. The graph in Figure 7 can be interpreted as asymptotically tending to linear T_S vs $\ln v$ representation at low scan rates. The slope of this representation (dotted line in Figure 7) is $16 \pm 1 \text{ V}^{-1}$. Inserting this value into eq 36 yields $\beta (= \alpha + n')$ = 0.41 ± 0.03 , a value near the typical values of this parameter (ca. 0.50).²

The nonlinear variation of T_S with $\ln v$, consistent with experimental data in Figures 2, 6, and 7, suggests that the g value approached by eq 33 is representative of the behavior at low scan rates but not of the voltammetric response at relatively high scan rates. One possible way to interpret this problem is to consider the presence of uncompensated ohmic drops in the cell. These effects can be significant in the case of gross microparticulate deposits of nonconducting materials, a frequent situation in VIMP experiments. Following the studies in solution phase⁴⁹ and surface-confined reactants,^{50,51} the current for a reversible electron transfer process can be rewritten as⁵²

$$i = \frac{nFv_{\text{eff}}\Gamma}{RT} \frac{\exp\left[\frac{nF}{RT}(E - E^\circ - ir_\Omega)\right]}{\left\{1 + \exp\left[\frac{nF}{RT}(E - E^\circ - ir_\Omega)\right]\right\}} \quad (37)$$

where r_Ω is the uncompensated ohmic resistance and v_{eff} is the effective potential scan rate defined as $v_{\text{eff}} = v + r_\Omega(di/dt)$. Following the same line of reasoning, one can rewrite eq 24 as

$$i = \frac{v_{\text{eff}}gq_0 e^{g(E-E^\circ-ir_\Omega)}}{[1 + e^{\gamma g(E-E^\circ-ir_\Omega)}]^{1/\gamma+1}} \quad (38)$$

Assuming that both the current and its variation with time are small (a situation reasonable at low scan rates), $v_{\text{eff}} \approx v$, a reasonable approximation for the Tafel-type relationship at the foot of the voltammetric wave is

$$i \approx \frac{vgq_0 e^{g(E-E^\circ)}}{1 + vg^2q_0r_\Omega e^{g(E-E^\circ)}} \quad (39)$$

In turn, when the applied potential is near the formal electrode potential

$$i \approx \frac{vgq_0[1 + g(E - E^\circ)]}{[1 + vg^2q_0r_\Omega]} \quad (40)$$

Finally, in the descending branch of the cathodic peak, $E \ll E^\circ$ and the current can be approached by the expression

$$i \approx \frac{vgq_0 e^{-\gamma g(E-E^\circ)}}{1 + \gamma vg^2q_0r_\Omega e^{-\gamma g(E-E^\circ)}} \quad (41)$$

For practical purposes, the most interesting result is that the Tafel-type relationship derived from eq 39,

$$\ln i \approx \ln \left[\frac{vgq_0}{1 + vg^2q_0r_\Omega e^{g(E-E^\circ)}} \right] + g(E - E^\circ) \quad (42)$$

significantly modifies that described by eq 28. A more detailed consideration of uncompensated resistive and capacitive effects expressed as a non-Faradaic current can be made following the classical treatment of Bard and Faulkner.⁵³ Interestingly, this treatment allows us to justify an experimental relationship reported for the reduction of mixed crystals of $\text{Cu}_x\text{Se}_{1-x}$ in contact with aqueous media to Cd metal:⁵⁴ the linear variation of peak potentials with the charge passed through the voltammetric peaks.

The non-Faradaic current associated with the double-layer charging and uncompensated resistance accompanying Faradaic processes occurring during an LSV experiment initiated at a given potential, E_s , can be expressed in terms of the differential equation:

$$E = E_s \pm vt = R \frac{dq}{dt} + \frac{q}{C} \quad (43)$$

where R and C represent, respectively, the uncompensated ohmic resistance and double-layer capacitance of the electrochemical cell. Then, the non-Faradaic current i_{NF} becomes,⁵³

$$i_{\text{NF}} = \left(\frac{E_s}{R} - vC \right) e^{-t/vRC} + vC \quad (44)$$

Assuming that the net current flowing through the cell is the sum of this current and the Faradaic component given by eq 24, one can write,

$$i = q_0g v \frac{e^{g(E-E^\circ)}}{[1 + e^{\gamma g(E-E^\circ)}]^{1/\gamma+1}} + vC + \left(\frac{E_s}{R} - vC \right) e^{-(E-E_s)/vRC} \quad (45)$$

The peak potential can be determined imposing the condition $di/dE = 0$, i.e.,

$$vq_0g^2e^{g(E_p-E^{\circ'})}[1-\gamma e^{\gamma g(E_p-E^{\circ'})}] - \left(\frac{E_s - vC}{vRC}\right)e^{-(E_p-E_s)/vRC} [1 + e^{\gamma g(E_p-E^{\circ'})}]^{1/\gamma+2} = 0 \quad (46)$$

Assuming that the peak potential is near the formal electrode potential, it is possible to take

$$vq_0g^2(1-\gamma) - \left(\frac{E_s - vC}{vRC}\right)e^{-(E_p-E_s)/vRC}2^{1/\gamma+2} = 0 \quad (47)$$

and, assuming that the $(E_p - E_s)/vRC$ ratio is small, it is possible to approximate

$$E_p = E_s + vRC \left[1 - \frac{v^2RCq_0g^2(1-\gamma)}{2^{1/\gamma+2}\left(\frac{E_s - vC}{vRC}\right)} \right] \quad (48)$$

In an LSV experiment performed at a potential scan rate v , this equation defines a linear relationship between E_p and q_0g^2 in agreement with experimental data reported by Meyer et al.⁵⁴ for the reduction of mixed crystals of $\text{CuS}_x\text{Se}_{1-x}$ in contact with aqueous media.

A second way to rationalize the obtained experimental results can be derived from the consideration of the peculiar nature of VIMP experiments. Here, typically, a set of particles micrometer-sized remains adhered to the graphite electrode surface. The deposit of solid particles can be described in terms of an array of interconnected microspheres or microcylinders fixed onto the electrode. Since the voltammetric process involves charge transport through a diffusion layer near the particles, this situation is to a great extent parallel to that described by Compton et al.⁸ on studying the voltammetry at porous electrodes. At low scan rates and/or small, well-separated particles, the solid deposit can be described as an array of microelectrodes displaying a thin-layer response. At high scan rates and/or large particles, the system behaves as a uniform deposit giving rise to a diffusive response. This is in turn qualitatively similar to that described by Murray et al.⁵⁵ for the solid-state voltammetry of polymer thin films on microdisk electrodes. Here, there is a transition from the thick film behavior to that described in terms of the summation of terms of thin-layer cell and microcylindrical geometries. The second component of the current is obtained by taking different values of the parameter $\gamma = nFr^2v/RTD$, where r denotes the radius of the microcylinders and D denotes the diffusion coefficient of the mobile ions permeating the polymer. Then, it is conceivable that the expression for the variation of g with the potential scan rate given by eq 33 must be modified to include any diffusive term whose importance will increase with v .

A third aspect to be considered is the possibility of different electrochemical mechanisms as described in Section 3.2. In principle, model I can be considered as dominating the voltammetric behavior at low scan rates, whereas model II should prevail at high scan rates. For the purpose of the unambiguous characterization of solid compounds, the relevant point to emphasize is that the described logistic approximation allows us to use the two phenomenological coefficients, g , γ (as well as their variation with potential scan rate) to characterize the solid. In fact, even at relatively large potential sweep rates at which the peaked response vanishes, the model satisfactorily

reproduces experimental LSVs as can be seen in Figure 8 for litharge in contact with 0.10 M H_2SO_4 at $v = 200 \text{ mV s}^{-1}$.

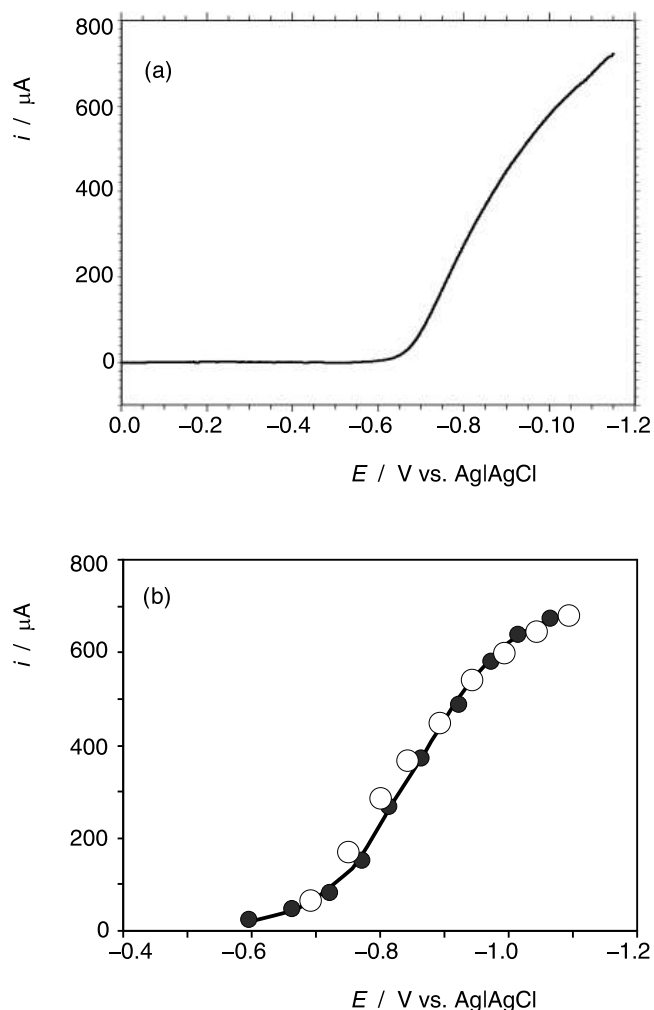


Figure 8. (a) LSV of litharge-modified graphite electrode in contact with 0.10 M H_2SO_4 at $v = 200 \text{ mV s}^{-1}$. (b) Superimposed experimental data points at selected potentials (circles) and theoretical (solid circles and continuous line) from eq 24 taking $E^{\circ'} = -0.77 \text{ V vs Ag/AgCl}$, $q_0gv = 1.0 \times 10^4 \mu\text{A}$; $g = -26.5 \text{ V}^{-1}$, $\gamma = 0.20$.

Interestingly, the model allows us to characterize different lead compounds even discriminating between different mineral forms of the same component (litharge and massicot for PbO) using the aforementioned parameters g and γ and the slope (T_s) and the ordinate at the origin (T_{00}) of the generalized Tafel-type representations as in Figure 6 at a given potential scan rate. Figure 9 depicts the LSVs recorded for graphite electrodes modified with (a) massicot, (b) lead-tin yellow (type II), (c) lead white, and (d) $\text{PbCl}_2 \cdot 2\text{H}_2\text{O}$, at a potential scan rate of 2 mV s^{-1} . The values of the material-characteristic parameters determined under these conditions are summarized in Table 1.

It is pertinent to note, however, that the logistic description of voltammetric curves in VIMP experiments proposed here involves a semiempirical approximation to a very complex problem. Accordingly, there is a need of clarifying the underlying physicochemical phenomena determining the electrochemistry of solid-to-solid transformations.

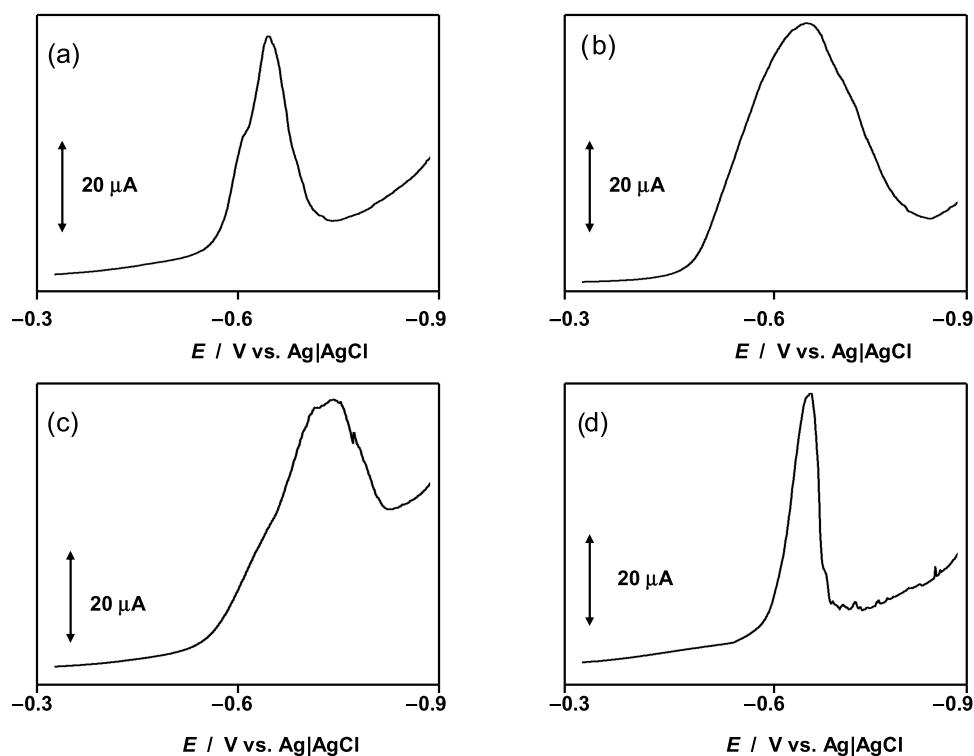


Figure 9. LSVs of graphite electrodes modified with (a) massicot, (b) lead-tin yellow (type II), (c) lead white, and (d) $\text{PbCl}_2 \cdot 2\text{H}_2\text{O}$, in contact with 0.10 M H_2SO_4 at $\nu = 2 \text{ mV s}^{-1}$.

Table 1. Peak Potentials (in mV vs Ag/AgCl), Logistic Parameters g , γ , and Slope (T_s) and Intercept (T_{00}) of the Tafel-Type Representations Determined from LSVs of the Studied Lead Compounds Attached to Graphite Electrodes in Contact with 0.10 M H_2SO_4 at a Potential Scan Rate of 2 mV s^{-1} ^a

solid	E_p	g (V^{-1})	γ	T_s (V^{-1})	T_{00}
litharge	-640 ± 5	-35 ± 1	1.0 ± 0.1	-34 ± 2	1.4 ± 0.2
massicot	-645 ± 5	-59 ± 1	1.0 ± 0.1	-59 ± 2	2.0 ± 0.3
lead-tin yellow II	-660 ± 5	-25 ± 1	0.8 ± 0.2	-29 ± 2	2.7 ± 0.3
lead white	-750 ± 10	-35 ± 1	0.6 ± 0.1	-24 ± 2	1.4 ± 0.2
naples yellow	-520 ± 10	-75 ± 3	0.9 ± 0.2	-68 ± 3	0.2 ± 0.2
$\text{PbCl}_2 \cdot 2\text{H}_2\text{O}$	-660 ± 5	-60 ± 2	1.5 ± 0.2	-54 ± 2	1.0 ± 0.2

^aAveraged data from three independent voltammetric measurements at freshly modified electrodes.

4. CONCLUSIONS

The well-known theory for the linear potential scan voltammetry of surface-confined reactants leads to current/potential curves, which can be reproduced assuming that the passed charge varies with the applied potential following a logistic growth. This idea was applied here to describe electrochemical processes involving the nontopotactic reduction of metal compounds to the corresponding metal in contact with aqueous electrolytes. These are frequent processes in the voltammetry of immobilized particles methodology of interest in the characterization of solid materials within a wide variety of contexts. The resulting semiempirical model allows us to construct current/potential curves introducing two phenomenological parameters whose values are dependent on the potential scan rate. Theoretical voltammograms are in close agreement with experimental ones recorded for different lead compounds attached to graphite electrodes in contact with 0.10 M H_2SO_4 aqueous solution in a relatively large interval of potential scan rates. The values of the phenomenological parameters, easily approximated using Tafel-

type representations, as well as their variation with potential scan rate can be used to characterize different solids.

AUTHOR INFORMATION

Corresponding Author

Antonio Doménech-Carbó – Department of Analytical Chemistry, Universitat de València, 46100 Burjassot, Valencia, Spain; orcid.org/0000-0002-5284-2811; Phone: +34-963544533; Email: antonio.domenech@uv.es; Fax: +34-963544436

Complete contact information is available at: <https://pubs.acs.org/10.1021/acs.jpcc.2c03041>

Notes

The author declares no competing financial interest.

ACKNOWLEDGMENTS

The work was carried out within the framework of project PID2020-113022GB-I00, which was financially supported by MCIN/AEI/10.13039/50110 0 011033.

REFERENCES

- (1) Brown, A. P.; Anson, F. C. Cyclic and Differential Pulse Voltammetric Behavior of Reactants confined to the Electrode Surface. *Anal. Chem.* **1977**, *49*, 1589–1595.
- (2) Laviron, E. General expression of the linear potential sweep voltammogram in the case of diffusionless electrochemical systems. *J. Electroanal. Chem.* **1979**, *101*, 19–28.
- (3) Honeychurch, M. J.; Rechnitz, G. A. Voltammetry of Adsorbed Molecules. Part 1: Reversible Redox Systems. *Electroanalysis* **1998**, *10*, 285–293.
- (4) Honeychurch, M. J.; Rechnitz, G. A. Voltammetry of Adsorbed Molecules. Part 2: Irreversible Redox Systems. *Electroanalysis* **1998**, *10*, 453–457.
- (5) Myland, J. C.; Oldham, K. B. Quasireversible cyclic voltammetry of a surface confined redox system: a mathematical treatment. *Electrochem. Commun.* **2005**, *7*, 282–287.
- (6) Eloul, S.; Compton, R. G. Charge Diffusion on the Surface of Particles with Simple Geometries. *J. Phys. Chem. C* **2015**, *119*, 27540–27549.
- (7) Martínez-Ortiz, F.; Laborda, E.; Limon-Petersen, J. G.; Rogers, E. I.; Serna, C.; Rees, N. V.; Molina, A.; Compton, R. G. Uptake of Molecular Species by Spherical Droplets and Particles Monitored Voltammetrically. *J. Phys. Chem. C* **2009**, *113*, 17215–17222.
- (8) Barnes, E. O.; Chen, X.; Li, P.; Compton, R. G. Voltammetry at porous electrodes: A theoretical study. *J. Electroanal. Chem.* **2014**, *720*–721, 92–100.
- (9) George, K.; van Berkel, M.; Zhang, X.; Sinha, R.; Bieberle-Hütter, A. Impedance Spectra and Surface Coverages Simulated Directly from the Electrochemical Reaction Mechanism: A Nonlinear State-Space Approach. *J. Phys. Chem. C* **2019**, *123*, 9981–9992.
- (10) Molina, A.; Gonzalez, J.; Henstridge, M.; Compton, R. G. Voltammetry of Electrochemically Reversible Systems at Electrodes of Any Geometry: A General, Explicit Analytical Characterization. *J. Phys. Chem. C* **2011**, *115*, 4054–4062.
- (11) Gonzalez, J.; López-Tenes, M.; Molina, A. Non-Nernstian Two-Electron Transfer Reactions for Immobilized Molecules: A Theoretical Study in Cyclic Voltammetry. *J. Phys. Chem. C* **2013**, *117*, 5208–5220.
- (12) Lancaster, M.; AlQurashi, A.; Selvakumar, C. R.; Maldonado, S. Quantitative Analysis of Semiconductor Electrode Voltammetry: A Theoretical and Operational Framework for Semiconductor Ultramicroelectrodes. *J. Phys. Chem. C* **2020**, *124*, 5021–5035.
- (13) Yang, M.; Compton, R. G. Voltammetry of Adsorbed Species: Nonideal Interactions Leading to Phase Transitions. *J. Phys. Chem. C* **2020**, *124*, 18031–18044.
- (14) Solano, F.; Inaudi, P.; Chiesa, M.; Kociok-Kohn, G.; Salvadori, E. D. C.; Vanossi, D.; Malandrino, M.; Carmieli, R.; Giacomino, A.; Fontanesi, C. Spin Multiplicity and Solid-State Electrochemical Behavior in Charge-Transfer Co-crystals of DBTTF/F4TCN. *J. Phys. Chem. C* **2021**, *125*, 8677–8683.
- (15) Scholz, F.; Meyer, B. Voltammetry of solid microparticles immobilized on electrode surfaces. In *Electroanalytical Chemistry, A Series of Advances*, Bard, A. J.; Rubinstein, I., Eds.; Marcel Dekker: New York, 1998; Vol. 20, pp 1–86.
- (16) Scholz, F.; Schröder, U.; Gulabowski, R.; Doménech-Carbó, A. *Electrochemistry of Immobilized Particles and Droplets*, 2nd ed.; Springer: Berlin-Heidelberg, 2014.
- (17) Doménech-Carbó, A.; Labuda, J.; Scholz, F. Electroanalytical chemistry for the analysis of solids: characterization and classification (IUPAC Technical Report). *Pure Appl. Chem.* **2012**, *85*, 609–631.
- (18) Lovrić, M.; Scholz, F. A model for the propagation of a redox reaction through microcrystals. *J. Solid State Electrochem.* **1997**, *1*, 108–113.
- (19) Oldham, K. B. Voltammetry at a three-phase junction. *J. Solid State Electrochem.* **1998**, *2*, 367–377.
- (20) Lovrić, M.; Hermes, M.; Scholz, F. The effect of the electrolyte concentration in the solution on the voltammetric response of insertion electrodes. *J. Solid State Electrochem.* **1998**, *2*, 401–404.
- (21) Lovrić, M.; Scholz, F. A model for the coupled transport of ions and electrons in redox conductive microcrystals. *J. Solid State Electrochem.* **1999**, *3*, 172–175.
- (22) Schröder, U.; Oldham, K. B.; Myland, J. C.; Mahon, P. J.; Scholz, F. Modelling of solid state voltammetry of immobilized microcrystals assuming an initiation of the electrochemical reaction at a three-phase junction. *J. Solid State Electrochem.* **2000**, *4*, 314–324.
- (23) González-Meza, O. A.; Larios-Durán, E. R.; Gutiérrez-Becerra, A.; Casillas, N.; Escalante, J. I.; Bárcena-Soto, M. Development of a Randles-Ševčík-like equation to predict the peak current of cyclic voltammetry for solid metal hexacyanoferrates. *J. Solid State Electrochem.* **2019**, *23*, 3123–3133.
- (24) Grygar, T. The electrochemical dissolution of iron(III) and chromium(III) oxides and ferrites under conditions of abrasive stripping voltammetry. *J. Electroanal. Chem.* **1996**, *405*, 117–125.
- (25) Grygar, T. Phenomenological kinetics of irreversible electrochemical dissolution of metal-oxide microparticles. *J. Solid State Electrochem.* **1998**, *2*, 127–136.
- (26) Jaworski, A.; Stojek, Z.; Scholz, F. A comparison of simulated and experimental abrasive stripping voltammetric curves of ionic crystals: reversible case. *J. Electroanal. Chem.* **1993**, *354*, 1–9.
- (27) Doménech-Carbó, A.; Doménech-Carbó, M. T.; Costa, V. Electrochemical methods in Archaeometry, Conservation and Restoration. In *Monographs in Electrochemistry Series*, Scholz, F., Ed.; Springer: Berlin-Heidelberg, 2009.
- (28) Doménech-Carbó, A.; Doménech-Carbó, M. T. Electroanalytical techniques in archaeological and art conservation. *Pure Appl. Chem.* **2018**, *90*, 447–462.
- (29) Doménech-Carbó, A.; Doménech-Carbó, M. T.; Peiró-Ronda, M. A. Dating archaeological lead artifacts from measurement of the corrosion content using the voltammetry of microparticles. *Anal. Chem.* **2011**, *83*, 5639–5644.
- (30) Doménech-Carbó, A.; Doménech-Carbó, M. T.; Capelo, S.; Pasies-Oviedo, T.; Martínez-Lázaro, I. Dating archaeological copper/bronze artifacts using the voltammetry of microparticles. *Angew. Chem., Int. Ed.* **2014**, *53*, 9262–9266.
- (31) Doménech-Carbó, A.; Scholz, F. Electrochemical age determinations of metallic specimens—the utilization of the corrosion clock. *Acc. Chem. Res.* **2019**, *52*, 400–406.
- (32) Verhulst, P.-F. Notice sur la loi que la population poursuit dans son accroissement. *Corresp. Math. Phys.* **1838**, *10*, 113–121.
- (33) Ausloos, M. Gompertz and Verhulst frameworks for growth and decay description. *Int. J. Comput. Anticip. Syst.* **2014**, *30*, 15–36.
- (34) Torresi, R. M.; Córdoba de Torresi, S. I.; Gonzalez, E. R. On the use of the quadratic logistic differential equation for the interpretation of electrointercalation processes. *J. Electroanal. Chem.* **1999**, *461*, 161–166.
- (35) Diard, J. -P.; Le Gorrec, B.; Montella, C. Logistic differential equation A general equation for electrointercalation processes? *J. Electroanal. Chem.* **1999**, *475*, 190–192.
- (36) Sadkowski, A. On the application of the logistic differential equation in electrochemical dynamics. *J. Electroanal. Chem.* **2000**, *486*, 92–94.
- (37) Hasse, U.; Scholz, F. In situ atomic force microscopy of the reduction of lead oxide nanocrystals immobilised on an electrode surface. *Electrochem. Commun.* **2001**, *3*, 429–434.
- (38) Gotor, F. J.; Criado, J. M.; Malek, J.; Koga, N. Kinetic Analysis of Solid-State Reactions: The Universality of Master Plots for Analyzing Isothermal and Nonisothermal Experiments. *J. Phys. Chem. A* **2000**, *104*, 10777–10782.
- (39) Doménech, A.; García, H.; Doménech-Carbó, M. T.; Llabrés-i-Xamena, F. Electrochemistry of Metal-Organic Frameworks: A Description from the Voltammetry of Microparticles Approach. *J. Phys. Chem. C* **2007**, *111*, 13701–13711.
- (40) Laviron, E. The Use of Linear Potential Sweep Voltammetry and of Ac Voltammetry for the Study of the Surface Electrochemical Reaction of Strongly Adsorbed Systems and of Redox Modified Electrodes. *J. Electroanal. Chem.* **1979**, *100*, 263–270.

(41) Doménech-Carbó, A. Rise and fall of historic tram networks: logistic approximation and discontinuous events. *Phys. A* **2019**, *522*, 315–323.

(42) Batchelor-McAuley, C.; Kätelhön, E.; Barnes, E. O.; Compton, R. G.; Laborda, E.; Molina, A. Recent Advances in Voltammetry. *ChemistryOpen* **2015**, *4*, 224–260.

(43) Tanner, E. E. L.; Barnes, E. O.; Tickell, C. B.; Goodrich, P.; Hardacre, C.; Compton, R. G. Application of Asymmetric Marcus–Hush Theory to Voltammetry in Room-Temperature Ionic Liquids. *J. Phys. Chem. C* **2015**, *119*, 7360–7370.

(44) Richards, F. J. A Flexible Growth Function for Empirical Use. *J. Exp. Bot.* **1959**, *10*, 290–300.

(45) Petrii, O. A.; Nazmutdinov, R. R.; Bronshtein, M. D.; Tisrlina, G. A. Life of the Tafel equation: Current understanding and prospects for the second century. *Electrochim. Acta* **2007**, *52*, 3493–3504.

(46) Doménech, A.; Doménech-Carbó, M. T.; Pasies-Oviedo, T.; Bouzas-Bello, M. C. Application of modified Tafel analysis to the identification of corrosion products on archaeological metals using voltammetry of microparticles. *Electroanalysis* **2011**, *23*, 2803–2812.

(47) Brainina, K. Z. *Stripping Voltammetry in Chemical Analysis*; Halsted: New York, 1974.

(48) Jones, S. E. W.; Toghill, K. E.; Zheng, S. H.; Morin, S.; Compton, R. G. The Stripping Voltammetry of Hemispherical Deposits Under Electrochemically Irreversible Conditions: A Comparison of the Stripping Voltammetry of Bismuth on Boron-Doped Diamond and Au(111) Electrodes. *J. Phys. Chem. C* **2009**, *113*, 2846–2854.

(49) Nicholson, R. S. Some Examples of the Numerical Solution of Nonlinear Integral Equations. *Anal. Chem.* **1965**, *37*, 667–671.

(50) Fan, F. R. F.; Mirkin, M. V.; Bard, A. J. Polymer Films on Electrodes. 25. Effect of Polymer Resistance on the Electrochemistry of Poly(vinylferrocene): Scanning Electrochemical Microscopic, Chronoamperometric, and Cyclic Voltammetric Studies. *J. Phys. Chem. A* **1994**, *98*, 1475–1481.

(51) Trijueque, J.; García-Jareño, J. J.; Navarro-Laboulais, J.; Sanmatias, A.; Vicente, F. Ohmic drop of Prussian-blue:graphite_epoxy electrodes. *Electrochim. Acta* **1999**, *45*, 789–795.

(52) Mircesky, V.; Lovrić, M. Ohmic drop effects in square-wave voltammetry. *J. Electroanal. Chem.* **2001**, *497*, 114–124.

(53) Bard, A. J.; Faulkner, L. R. *Electrochemical Methods*; John Wiley & Sons: New York, 1980.

(54) Meyer, B.; Zhang, S.; Scholz, F. The quantitative analysis of mixed crystals $\text{Cu}_x\text{Se}_{1-x}$ with abrasive stripping voltammetry and a redetermination of the solubility product of CuSe and the standard potential of the Cu/CuSe electrode. *Fresenius J. Anal. Chem.* **1996**, *356*, 267–270.

(55) Geng, L.; Reed, R. A.; Longmire, M.; Murray, R. W. Solid-State Linear Sweep Voltammetry. A Probe of Diffusion in Thin Films of Polymer Ion Conductors on Microdisk Electrodes. *J. Phys. Chem. B* **1987**, *91*, 2908–2914.

Recommended by ACS

Evaluating Analytical Expressions for Scanning Electrochemical Cell Microscopy (SECCM)

Kamsy Lerae Anderson and Martin Andrew Edwards

MAY 16, 2023
ANALYTICAL CHEMISTRY

READ 

Finite Element Modeling of the Combined Faradaic and Electrostatic Contributions to the Voltammetric Response of Monolayer Redox Films

Katherine J. Levey, Julie V. Macpherson, *et al.*

SEPTEMBER 07, 2022
ANALYTICAL CHEMISTRY

READ 

A Refined Redox Titration Simulation Program for the Simple System

Qiang Fu, Shiyuan Fu, *et al.*

MAY 08, 2023
JOURNAL OF CHEMICAL EDUCATION

READ 

Electrochemical Heterogeneity at the Nanoscale: Diffusion to Partially Active Nanocubes

Rachel Wong, Richard G. Compton, *et al.*

AUGUST 12, 2022
THE JOURNAL OF PHYSICAL CHEMISTRY LETTERS

READ 

Get More Suggestions >